Applied Catalysis B: Environment and Energy 353 (2024) 124076

Contents lists available at ScienceDirect

Applied Catalysis B: Environment and Energy

journal homepage: www.elsevier.com/locate/apcatb

Modulating the electronic structures of Fe_3C-based catalyst by surface sulfidation to facilitate H_2O_2 activation

Dunyu Sun [a], Leliang Wu [a], Qiang Zhong [a,b], KwangChol Ri [a,d], Syed Azhar Abbas [a], Shaogui Yang [a,c,*], Chenmin Xu [a,**], Shanshan Ding [e], Yazi Liu [a], Zhe Xu [a], Chengdu Qi [a], Huan He [a], Shiyin Li [a], Cheng Sun [f]

[a] School of Environment, Jiangsu Province Engineering Research Center of Environmental Risk Prevention and Emergency Response Technology, Jiangsu Engineering Lab of Water and Soil Eco-remediation, Nanjing Normal University, Nanjing 210023, PR China
[b] School of Geography, Nanjing Normal University, Nanjing, Jiangsu 210023, PR China
[c] Suzhou Furong Environmental Engineering Co., Ltd, Suzhou 215500, PR China
[d] Institute of Chemical Engineering, Hamhung University of Chemical Engineering, Hamhung, Democratic People's Republic of Korea
[e] Australian Institute for Bioengineering and Nanotechnology, The University of Queensland, St Lucia, Brisbane, QLD 4072, Australia
[f] State Key Laboratory of Pollution Control and Resource Reuse, School of Environment, Nanjing University, Nanjing, Jiangsu 210023, PR China

ARTICLE INFO

Keywords:
Sulfidation
FeS_2
Heterogeneous Fenton
Mechanism

ABSTRACT

The performance of Fe-based heterogeneous Fenton catalysts is apparently affected by the electron density of Fe active site. Herein, we modulate the active site electronic density of the Fe_3C-based catalyst by surface sulfidation to improve H_2O_2 activation property. After sulfidation, the removal of acetaminophen (APAP) increased from 27.1% to 100%, and the degradation rate constant k_{obs} of APAP increased 5.44-fold. Sulfidation enhances the utilization of H_2O_2 and improves the generation of active species. Theoretical calculations demonstrated that sulfidation increases the electron density of Fe sites and lowers the band gap between the d-band center and Fermi energy level, facilitating electron transfer and H_2O_2 activation. The change in cleavage position of H_2O_2 from O-H to O-O after sulfidation provides additional evidence for the increased generation of •OH. These results elucidate the promoting effect of sulfidation on heterogeneous Fenton catalysts and provide a strategy for improving the performance of catalyst and contaminant removal.

1. Introduction

Fenton reaction is one of the most popular and effective water treatment technologies over the last hundred years [1–4]. The removal of pollutants by the Fenton reaction relies on hydroxyl radicals (•OH) generated by the reaction between ferrous and hydrogen peroxide (H_2O_2) (Eq.1) [5–7]. Subsequently, the formed ferric was reduced to ferrous by reacting with H_2O_2 (Eq.2), which accomplished the valence cycle of Fe [8,9]. However, due to the pH sensitivity of ferrous in aqueous solution, the narrow pH range and copious residual sludge limit the application of the Fenton reaction [10,11]. To overcome these drawbacks, a heterogeneous Fenton reaction has been proposed using solid catalysts instead of iron ions [12–14]. Different from homogeneous Fenton, the heterogeneous Fenton process is more complex, involving the adsorption, activation, and desorption of H_2O_2 and target pollutants [15]. In this, the activation of H_2O_2 is a crucial step that determines the removal efficiency of pollutants. During H_2O_2 activation, the electron transfer from the Fe active site of catalysts to H_2O_2 and induces O-O breaking and •OH generation [7]. The electron density of Fe site is a crucial factor for H_2O_2 activation during heterogeneous Fenton reaction [16]. For example, the Fe site of iron carbide (Fe_3C), which has a low electron density, tends to accept electrons from H_2O_2 to form $O_2^{\bullet-}$ (-0.33 V vs. SHE) instead of •OH (2.38 V vs. SHE), resulting in unsatisfactory pollutant removal performance [6,7,17]. Therefore, modulating the electron density of the Fe active site is an effective strategy to improve heterogeneous Fenton performance.

$$Fe(II) + H_2O_2 \rightarrow \bullet OH + Fe(III) + OH^- \; k = 40 - 80 M^{-1} S^{-1} \quad (1)$$

* Corresponding author at: School of Environment, Jiangsu Province Engineering Research Center of Environmental Risk Prevention and Emergency Response Technology, Jiangsu Engineering Lab of Water and Soil Eco-remediation, Nanjing Normal University, Nanjing 210023, PR China.
** Corresponding author.
E-mail addresses: yangsg@njnu.edu.cn (S. Yang), chenmin_xu@163.com (C. Xu).

https://doi.org/10.1016/j.apcatb.2024.124076
Received 11 January 2024; Received in revised form 10 April 2024; Accepted 13 April 2024
Available online 16 April 2024

$$Fe(III) + H_2O_2 \rightarrow Fe(II) + \bullet O_2H / \left(O_2^{\bullet -} + H^+\right)\ k = 9.1 \times 10^{-7}\ M^{-1}\ S^{-1} \quad (2)$$

Currently, complexing agents, reductants, and co-catalysts are commonly used to modulate Fe surrounding electron density and improve the catalytic performance of heterogeneous Fenton reactions [18–21]. However, the addition of complexing agents or reductants tends to increase the leaching of metal ions and compete with pollutants for active species, resulting in secondary pollution and unsatisfactory pollutant removal efficiency [22,23]. In contrast, co-catalyst loading has become a potential measure to regulate active site electronic structures due to appropriate electron distribution and few self-quenching effects [19,20]. Common co-catalysts include metal oxides such as CuO, metal sulfides such as MoS_2, etc. [24–26]. Zuo et al. utilized CuO to construct a built-in electric field to modulate FeOCl electron density and regulate the generation of active species [27]. Moreover, MoS_2 also can modulate the electron density of MIL-101(Fe) by S vacancy and promote peroxide activation for pollutant removal [28]. Meanwhile, the S sites serve as a rich electronic center to continuously donate electrons during the activation process [29]. However, the electron density modulation by combining with co-catalysts is limited by the finite composite interface as well as significant electron transfer losses [29]. Therefore, the integrated electron structure modulation of heterogeneous Fenton catalysts needs to be further developed.

Sulfidation is an efficient surface modulation measure by forming a sulfide layer on the surface of catalysts [30]. Previous studies have demonstrated that the surface physicochemical structure such as hydrophobicity, electron transfer, reactivity and selectivity of Fe-based catalysts can be controlled by sulfur loading [30–32]. Furthermore, the formation of FeS_x coating layer on the catalyst surface by sulfidation can regulate the surface oxygen-containing functional groups and specific surface area, thereby tuning the adsorption and activation of target substances and facilitating catalytic reactions [33–35]. In the heterogeneous Fenton process, sulfidation enhances the H_2O_2 activation performance of catalysts by lowering the pH of aqueous solution [36]. Moreover, the introduced sulfur species serve as electron donors and electron shuttles to efficiently convert Fe(III) to Fe(II), facilitating the generation of •OH [37]. Although sulfidation apparently promotes the heterogeneous Fenton performance of the Fe-based catalysts, few studies have focused on the alteration of electronic structure triggered by sulfidation, which is crucial for H_2O_2 activation. Therefore, further investigation and clarification are required to reveal the alteration of electronic structure and the impact of H_2O_2 activation triggered by sulfidation.

Herein, we utilized robust Fe_3C as a heterogeneous Fenton catalyst to investigate the impact of sulfidation on the catalyst's electronic structure and H_2O_2 activation property. The FeS_2 in situ formed on the surface of the Fe_3C-based catalyst was synthesized by the pyrolysis and sulfation of Prussian white (PW). Acetaminophen (APAP), a typical nonsteroidal anti-inflammatory drug and high-risk organic pollutant, was used as a model contamination to evaluate the heterogeneous Fenton performance of different catalysts, while H_2O_2 utilization was calculated to access the catalyst reactivity. The active species generated in the different systems were identified by quenching experiments, probe experiments, and electron paramagnetic resonance (EPR). In addition, the degradation intermediates were identified by high-performance liquid chromatography-tandem mass spectrometry (HPLC-MS). The mechanism of catalytic reaction and APAP degradation was elucidated by combining experiment and theoretical calculation. Moreover, the durability, stability, reliability, and safety of sulfation were evaluated by cycle experiment, long-term performance experiment, and intermediates toxicity calculation, respectively. This study sheds light on the enhancement mechanism of sulfation in heterogeneous Fenton reactions and provides an efficient measure to increase the catalyst activity.

2. Materials and methods

2.1. Chemical reagents

Detailed information on the purity and manufacturers of the chemical reagents used in this work is provided in **Text S1**.

2.2. Synthesis of PW, Fe_3C/NCT, and FeS_2/Fe_3C/NCT

2.2.1. Prussian white and Fe_3C/NCT

Prussian white ($Na_{3.1}Fe_4[Fe(CN)_6]_3$, PW) with a tubular structure was fabricated by a facile self-template method. First, $Na_4Fe(CN)_6{\cdot}10H_2O$ (0.45 g) was dissolved in 56 mL of ethylene glycol with stirring for 20 min to obtain a mixed solution. Then, 3 g of ascorbic acid was added to the solution and stirred for a further 30 min. Finally, the mixed solution was transferred to 100 mL Teflon-lined autoclaves and aged for 24 h at 70°C. After cooling down to approximately 25°C, the precursor was collected and washed several times with ethanol. The washed samples were then dried in a vacuum oven at 60°C overnight. After these operations, the tubular PW was obtained. Fe_3C embodied on tubular N-loaded carbon materials (NCT) was fabricated by a pyrolysis method after mixing with glucose. Simplify, the same mass of PW and glucose was mixed by grinding in an agate mortar, and heated to 550°C for 180 min in an N_2 atmosphere at a heating rate of 5°C/min. Fe_3C/NCT (denoted as FNC) was obtained after washing with ethanol and deionized water and dried in a vacuum oven at 60°C overnight.

2.2.2. FeS_2/Fe_3C/NCT

FeS_2/Fe_3C/NCT (FSNC) was fabricated by a sulfidation method. First, the prepared Fe_3C/NCT and sulfur powder with different mass ratios (1:3, 1:5, and 1:7) were placed at opposite corners of the alumina cube. Then, the cube was placed in a tube furnace and sulfidation at 350°C for 60 min at a heating rate of 5°C/min. After cooling to approximately 25°C, the samples were washed with ethanol and water, and dried in a vacuum oven at 60°C overnight. The successfully fabricated FSNC using different mass ratios (1:3, 1:5, and 1:7) were designated as FSNC-x (x=3, 5, and 7), respectively. Similarly, S-Fe_3O_4 was fabricated by the same method only replacing FNC with Fe_3O_4, and the preparation method of Fe_3O_4 was shown in the Text. S2.

2.3. Characterization

The X-ray diffractometer (XRD, D/Max 2500) with Cu Kα radiation was conducted to identify the crystalline phase of the synthesized catalysts. High-resolution scanning electron microscope (HRSEM, Apreo 2 S, Thermo Fisher Scientific Ltd., USA) and high-resolution transmission electron microscope (HRTEM, JEM-2100 F, JEOL Ltd., Japan) with X-ray spectroscopy (EDS) were applied to visualize the microscopic morphology and elemental composition of the catalysts. X-ray photoelectron spectroscopy (XPS, ESCALAB Xi+, Thermo Fisher Scientific Ltd., USA), Raman spectra (Raman, LabRAM HR800, HORIBA Jobin Yvon, French) and Fourier transform infrared spectra (FT-IR, Nicolet IS5, Thermo, USA) were employed to analyze chemical state and composition and functional group of synthesized catalysts. The specific surface areas were calculated by the N_2 adsorption-desorption isotherm (BET, BELSORP-mini X, Micotrac, Japan) in a relative pressure ranging from 0.0 to 1.0. The fluorescence intensity of the probe compound was detected using a fluorescence spectrophotometer (Lumina, Thermo-Fisher, USA).

2.4. Degradation experiment

Degradation experiments were performed in 100 mL beakers containing 50 mL of 10 mg/L APAP solution and magnetically stirred at room temperature with 500 rpm. The degradation reaction was initiated by the sequential addition of 5 mM H_2O_2 and 0.2 g/L catalyst. At

predetermined time intervals, 0.8 mL solution samples were extracted from the solutions, then filtered and quenched with a polytetrafluoroethylene syringe filter (PTFE, 0.22 μm) and 200 μL methanol. In quenching experiments, overdosage quenchers such as tert-butylalcohol (TBA), methanol (MeOH), 1,4-benzoquinone (BQ), and L-histidine (L-his) were used to identify the active species in the reaction. Terephthalic acid (TA), nitrotetrazolium blue chloride (NBT), and phenyl methyl sulfoxide (PMSO) was added as probes to identify specific active species. All the experiments were performed in duplicate to ensure the reproducibility of the results.

2.5. Analytical and calculation methods

The concentrations of APAP, PMSO, phenyl methyl sulfone ($PMSO_2$), tetracycline (TC), phenol, and sulfamethoxazole (SMX) were determined by high-performance liquid chromatography (HPLC) (Agilent 1290) equipped with a C18 column (150 mm) and detected by a diode array detector (DAD), and detailed information can be seen in Table S1. Residual H_2O_2 concentrations were detected by the Ti(IV) colorimetric method (**Text S3**). Furthermore, the formed •OH, $O_2^{\bullet-}$ were detected by probe experiments with TA and NBT, respectively (**Text S4**). The leached Fe concentrations were detected by the 1,10-phenanthroline method. In addition, the reactive oxygen species (ROSs) in the NCF-8/H_2O_2 system were identified by quenching with TBA, MeOH, BQ, and L-his followed by EPR using DMPO and TEMP as the spin trapping agents. The APAP degradation intermediates were identified by HPLC combined with a mass spectrometer (HPLC-MS, Thermo Scientific, US) coupled with a C18 column (see detailed information in **Text S5**). The methods of electrochemical analysis and theoretical calculation were described in **Text S6** and **Text S7.**

Based on the experimental data, the degradation rate constant k was computed by the pseudo-first-order kinetic model as described in the following Eq. (3). The H_2O_2 utilization ratio η was calculated by dividing depletion concentration by the addition concentration of H_2O_2 (Eq. (4)) [38]. The degradation performance of APAP in the different systems was calculated based on the removal of APAP, the usage of catalysts and oxidants, and the time spent (**Text S8**).

$$-\ln\left(\frac{C_t}{C_0}\right) = kt \tag{3}$$

$$\eta = \frac{C_{depletion}}{C_{addition}} \times 100\% \tag{4}$$

where C_0 (mg/L) and C_t (mg/L) are the APAP concentrations at the original and different reaction time (t, min), k (min^{-1}) is the apparent reaction rate constant, and $C_{depletion}$ and $C_{addition}$ are the consumed and added H_2O_2 concentrations.

3. Results and discussion

3.1. Characterization

As illustrated in Fig. 1**a**, the FNC and FSNC were successfully synthesized by pyrolysis and sulfidation. From the XRD spectra, the

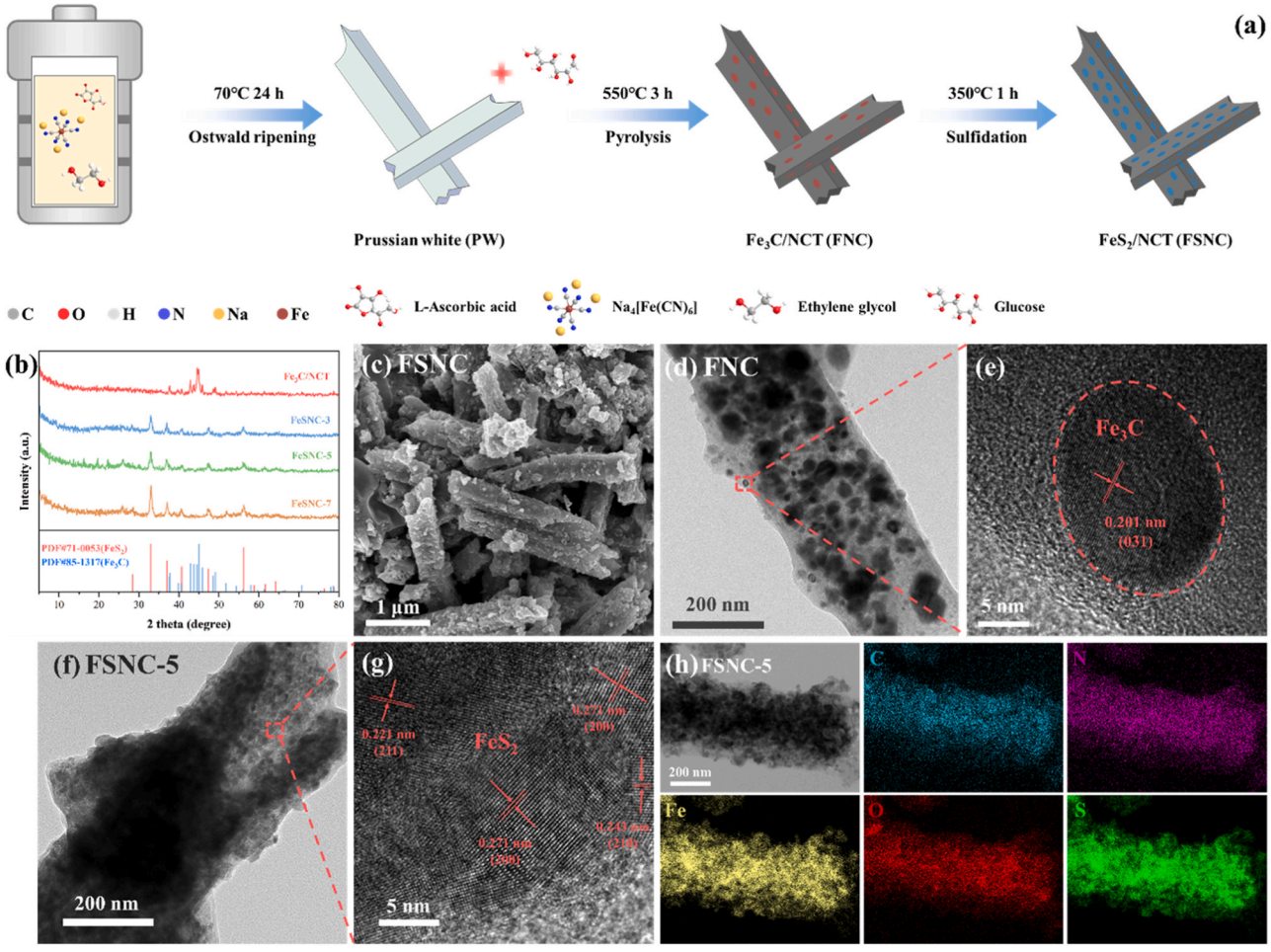

Fig. 1. Schematic diagram of catalyst synthesis (a), the XRD spectra of different catalysts (b), SEM image of FNC FSNC-5 (c), HRTEM imager of FNC (d-e) and FSNC-5 (f-g) and element mapping of FSNC-5 (h).

diffraction peaks at 37.71°, 42.79°, 44.63°, and 45.82° are ascribed to the (210), (211), (031) and (112) planes of Fe_3C (PDF#85–1317), respectively **(**Fig. 1**b)** [39]. The new peaks appearing at 32.87°, 36.98°, 40.53°, 47.40°, and 56.27° after sulfidation are ascribed to the (200), (210), (211), (220), and (311) planes of FeS_2 (PDF#71–0053), respectively [40]. Notably, the characteristic peak intensity of FeS_2 was significantly enhanced with the increase of S powder, suggesting that the formation of FeS_2 is correlated with the addition of sulfur powder. The SEM image of FNC displayed a rough square tube morphology with a length of 2–3 μm and a width of 400 nm **(**Fig. S1**)**. In comparison, FSNC-5 shows no significant change, only an increase in roughness (Fig. 1**c**), suggesting that sulfidation has a negligible effect on the catalyst morphology. As shown in Fig. 1**d-e**, Fe_3C nanoparticles were uniformly dispersed on the tube and exposed with (031) crystalline plane. After sulfidation, the nanoparticles were converted to FeS_2 with the (211), (200), and (210) crystalline planes, indicating that FeS_2 is the major form of Fe on the catalyst surface (Fig. 1**f-g**). Moreover, element mapping of FSNC-5 reflected that C, N, Fe, O, and S atoms are uniformly distributed on the tubular structure with a S/Fe mass ratio of 0.83 (Fig. 1**h** and Fig. S2).

As shown in Fig. 2**a**, the peaks at 3425 cm^{-1}, 1628 $cm^{-1,}$ and 594 cm^{-1} in the FTIR spectra corresponded to the stretching vibration of O–H, C═C, and Fe–O, respectively [29]. Notably, new peaks at around 1200 cm^{-1}-1000 cm^{-1} and 423 cm^{-1} appeared after sulfidation, corresponding to the stretching vibration of C-S and Fe-S, further confirming the successful loading of S atoms [41]. Compared to FNC, the I_D/I_G of FSNC-5 increased from 0.729 to 0.943, indicating that sulfidation reduces the degree of defects in carbon carriers (Fig. 2**b**). However, the specific surface area of FNC is 313.79 m^2/g and decreased to 50.26 m^2/g after sulfidation while the pore diameter was slightly changed, which may be due to the pore filling by the introduced S atom (Fig. 2**c** and Table S2). The distinct characteristic peak of S in the XPS spectra demonstrated the successful introduction of S atoms (Fig. 2**d**). In the C 1s spectra, the peaks at 284.78 eV, 285.48 eV and 288.66 eV correspond to C═C, C–O/C–C, and C═O [38], respectively, and show no significant alteration after sulfidation, suggesting that sulfidation does not affect the carbon carrier (Fig. S3). However, the intensity of O increases dramatically after sulfidation, which is attributed to the raised intensity of –OH at 533.04 eV and O_{ads} (adsorbed oxygen) at 531.97 eV, and the weakened intensity of O_{latt} (lattice oxygen) at 503.31 eV, indicating that S substitutes partial lattice O and provides additional adsorption sites to facilitate oxygen atom adsorption (Fig. S4) [42]. Meanwhile, a clear and sharp peak appeared at 707.49 eV, which can be assumed to FeS_2, demonstrating that the introduction of S element significantly reduces Fe valence and increases electron density during catalyst synthesis (Fig. 2**e**) [43]. The introduced S atoms are mainly present in the form of S^{2-}, S_2^{2-} and SO_x^{2-}, resulting from the peaks at 162.79 eV, 163.92 eV, 165.02 eV and 169.18 eV in the S 2p spectra (Fig. 2**f**) [37,44] . FeS_2 was formed when Fe bonds with S in the form of S_2^{2-}. The S^{2-} can be attributed to the intermediate FeS formed during the conversion of Fe_3C to FeS_2, which does not show a distinct crystalline phase [30]. In addition, the presence of SO_x^{2-} can be attributed to the complex of the sulfur and oxygen atoms formed by the oxidation of the catalyst during storage. Based on the above characterization results, it can be found that the Fe_3C on catalyst surface was converted to FeS_2. Since Fe_3C is a relatively stable material and Fe_3C diffraction signal is present in the XRD spectra after etching (Fig. S5), we suppose that the bottom layer of the post-sulfidation FSNC-5 is still Fe_3C and the surface layer is FeS_2.

3.2. Catalytic performance

The removal of APAP was adapted to evaluate the catalytic activity of different catalysts. As shown in Fig. 3**a**, APAP has little removal in the presence of H_2O_2 alone and 27.1 % APAP was removed in the FNC/H_2O_2 system, indicating that the oxidizing capacity of H_2O_2 itself and activated by FNC is not sufficient to remove APAP. Whereas, almost 100 % of APAP was removed in the FSNC/H_2O_2 system while the contribution of adsorption was only 5 %. Furthermore, the removal of APAP was raised with the increasing addition of S powder in the synthesis process, suggesting that the catalytic performance is affected by the amount of FeS_2 generated and shows a positive correlation. The dramatically reduced specific surface and unappreciable changed

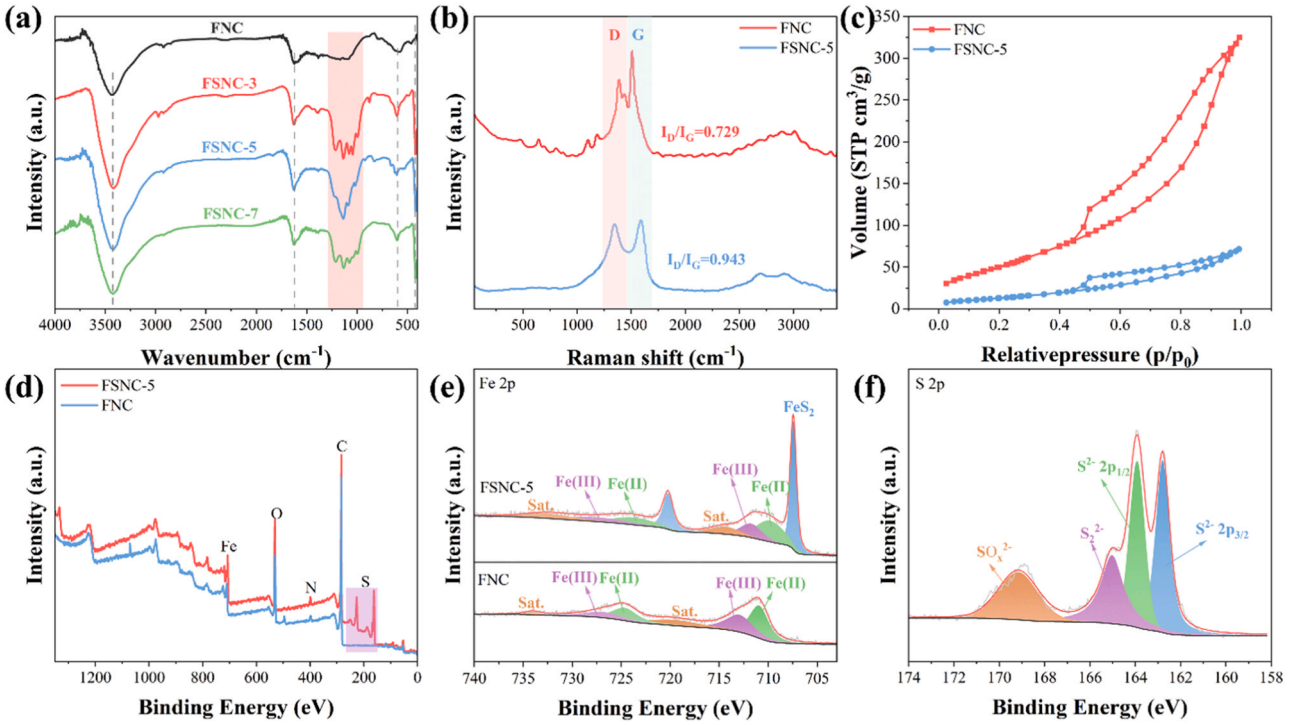

Fig. 2. The FTIR spectra (a), Raman spectra (b), N_2 adsorption-desorption isotherm (c), XPS spectra (d), and Fe 2p spectra (e) of FNC and FSNC, and S 2p spectra of FSNC-5 (f).

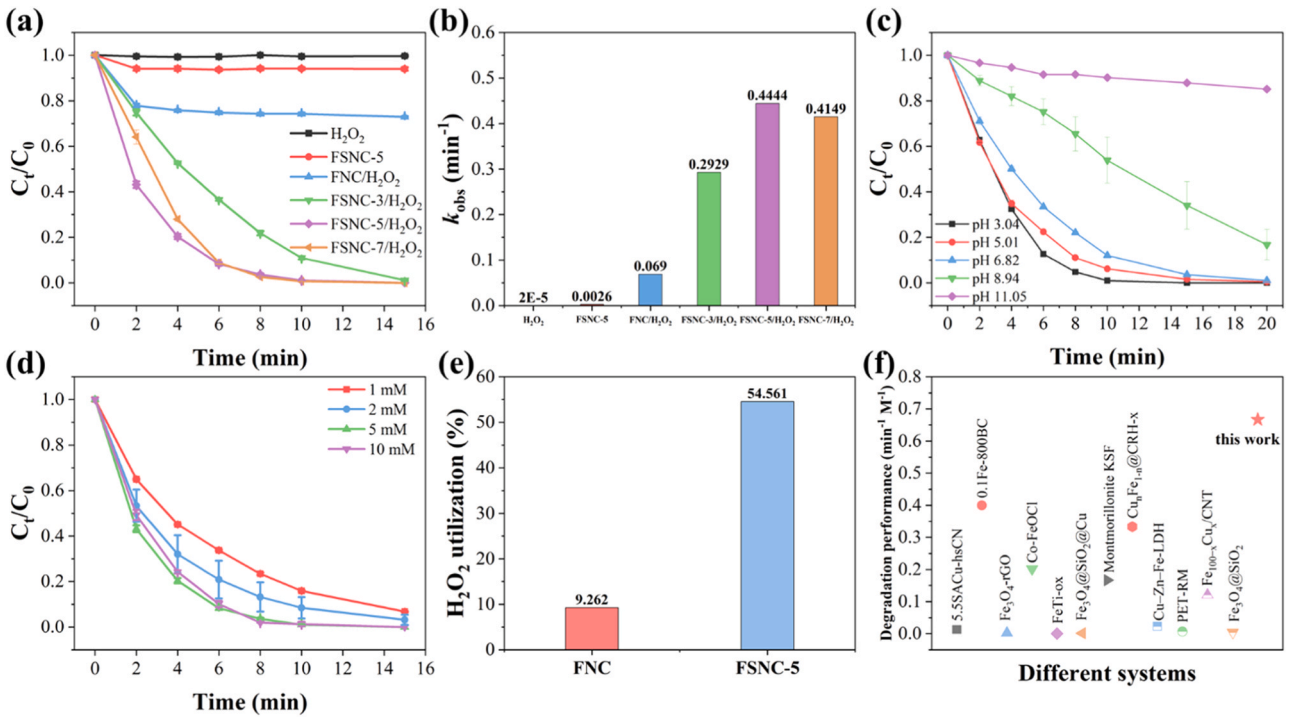

Fig. 3. The removal of APAP in different systems (a) and its degradation rate constant *k* (b), the effect pH (c) and H_2O_2 concentration (d) on APAP removal in the FSNC-5/H_2O_2 system, H_2O_2 utilization of FNC and FSNC-5 (e) and comparison of APAP degradation performance for different catalysts in H_2O_2 activation (f). [Experiment condition: 0.2 g/L catalysts, 5 mM H_2O_2, pH 5.86, 10 mg/L APAP].

surface functional group demonstrated that they do not contribute to the removal of APAP. The APAP degradation rate constants (k_{obs}) in different systems were calculated and shown in Fig. 3**b**. Notably, the k_{obs} of APAP in the FSNC-5/H_2O_2 system was 0.44 min^{-1}, which was 5.44 times higher than that in the FNC/H_2O_2 system. These results demonstrate that sulfidation significantly enhances the removal of APAP. In addition, pH, as a crucial factor in the Fenton reaction, was invested in evaluating its effect in the FSNC/H_2O_2 system, and APAP removal decreased with the increasing initial pH value (Fig. 3**c**). APAP can almost be removed when the initial pH below 6.82 and reduce to 83.2 % at pH 8.94. Meanwhile, the final pH after the reaction decreased to approximately 3.5, which increased the oxidation potential of •OH (Fig. S6). However, the removal of APAP was only 14.9 % at pH 11.05 and the final pH only dropped to 9.7, which may be due to the •OH eliminated by excess OH^- in the solution at high pH [11]. In addition, the removal of APAP increased when the initial H_2O_2 concentration was below 5 mM, and slightly decreased at 10 mM (Fig. 3**d**). Similarly, the H_2O_2 decomposition rate constant k_{obs} increased rapidly and then leveled off with increasing initial H_2O_2 concentration (Fig. S7 **a** and **b**). During the reaction, only 9.3 % of H_2O_2 was decomposed by FNC while the H_2O_2 decomposition ratio reached 54.6 % in the FSNC-5/H_2O_2 system, suggesting that FSNC-5 exhibited a greater ability to activate H_2O_2 compared to FNC (Fig. S8 and Fig. 3**e**). By comparing the performance of different heterogeneous catalysts for the degradation of APAP by activating H_2O_2, it can be found that the FSNC exhibits excellent APAP degradation performance (Fig. 3**f** and Table S3).

3.3. ROSs identification

Active species play a crucial role in the decontamination activity and pathway. TBA, MeOH, p-BQ, and L-his were used as the quenchers of •OH, $SO_4^{\bullet-}$, $O_2^{\bullet-}$, and $^1O_2$ to preliminarily and adequately identify potential active species in the FSNC-5/H_2O_2 system [45]. APAP removal was inhibited to 65.3 %, 46.1 %, 39.8 %, and 18.3 % after the addition of p-BQ, TBA, MeOH, and L-his, respectively, indicating that •OH is the major active species in the FSNC-5/H_2O_2 system and the contribution of $SO_4^{\bullet-}$ and $O_2^{\bullet-}$ can be ignored (Fig. 4**a**). PMSO was used as a probe to analyze whether Fe^{IV}=O was generated in the FNC/H_2O_2 and FSNC-5/H_2O_2 systems [46]. Although the concentration of PMSO was significantly reduced from 83.93 μM to 3.71 μM in the FSNC-5/H_2O_2 system and to 78.82 μM in the FNC/H_2O_2 system with no $PMSO_2$ was formed in both systems, suggesting that Fe^{IV}=O is not the active species in both systems (Fig. 4**b**).

To further investigate the alteration of reactive species before and after sulfidation, EPR and probe experiments were used to identify the major active species in both systems. As shown in Fig. 4**c**, the only distinct quartet signal with A_N=A_H=14.9 corresponded to DMPO-•OH, suggesting that •OH was generated in both FNC/H_2O_2 and FSNC-5/H_2O_2 systems without $SO_4^{\bullet-}$ formation [47]. Higher DMPO-•OH signal intensity in the FSNC-5/H_2O_2 system suggests that the formation of •OH increased dramatically after sulfidation [48]. Furthermore, TA was used as a probe to detect formed •OH in both systems, which can easily react with •OH to form 2-hydroxyterephthalic acid (HTA) with a strong photoluminescence (PL) signal [49]. The distinct increase in PL signal intensity of HTA occurred in the FSNC-5/H_2O_2 system but no significant change in intensity was detected in the FNC/H_2O_2 system. Consistent with the EPR result, this finding further verifies that sulfidation facilitates the generation of •OH (Fig. 4**d**). Similarly, the signal at A_N=14 G and A_H=10 G was consistent with the signal of DMPO-$O_2^{\bullet-}$, and the intensity of DMPO-$O_2^{\bullet-}$ in the FSNC-5/H_2O_2 system was greater than that in the FNC/H_2O_2 system, suggesting that $O_2^{\bullet-}$ was generated in both systems and that sulfidation also facilitates $O_2^{\bullet-}$ formation (Fig. 4**e**) [47]. To further verify this finding, the NBT was used as a probe to indirectly detect the concentration of $O_2^{\bullet-}$ in both systems [50]. Notably, the absorbance of NBT in the FSNC-5/H_2O_2 system decreased more significantly than that in the FNC/H_2O_2 system while the removal of NBT by FNC adsorption was higher than that of FSNC (Fig. 4**f** and **S9**). This result further confirms that more $O_2^{\bullet-}$ was generated during the activation of H_2O_2 by the catalyst after sulfidation. However, these $O_2^{\bullet-}$ did not significantly contribute to APAP degradation. Furthermore, the distinct

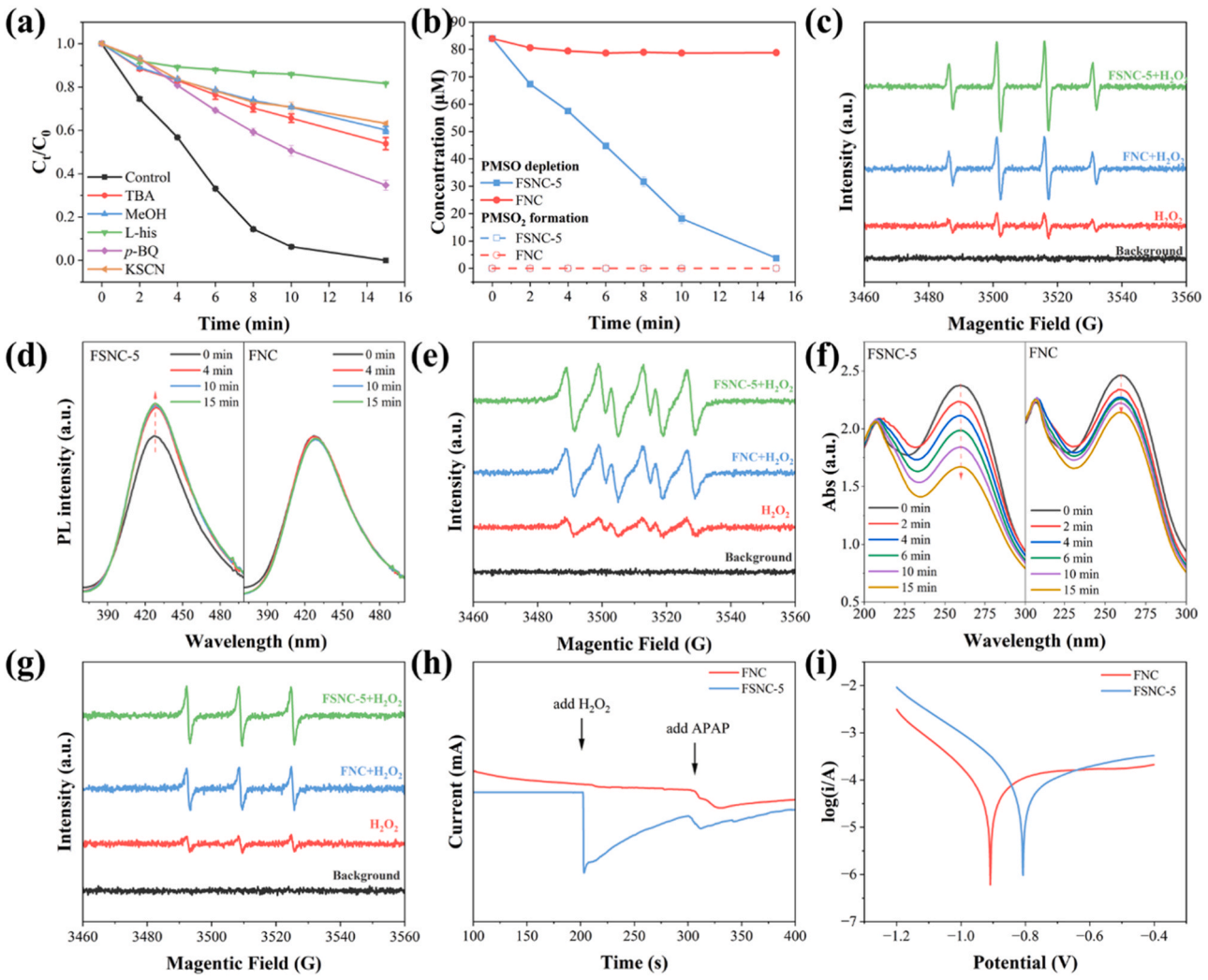

Fig. 4. The quenching experiment with different quenchers (a), the concentration of PMSO depletion and $PMSO_2$ formation (b), EPR detection for •OH (c), the photoluminescence intensity of formed HTA (d), EPR signal of $O_2^{\bullet-}$ (e), the absorbance NBT in different systems (f), EPR signal of $^1O_2$ (g), the current change after adding H_2O_2 or APAP (h) and Tafel curve of FNC and FSNC-5 (i). [Experiment condition: 0.2 g/L catalysts, 5 mM H_2O_2, pH 5.86, 10 mg/L APAP, 100 mM TBA and MeOH, 20 mM KSCN, 10 mM L-his, 5 mM p-BQ, 0.1 mM PMSO and TA, and 0.05 mM NBT].

triple signal intensity of 1:1:1 was consistent with TEMP-$^1O_2$, demonstrating that $^1O_2$ was generated in both systems (Fig. 4**g**). Compared to the FNC/H_2O_2 system, the intensity of TEMPO-$^1O_2$ increased, suggesting that post-sulfide FSNC-5 generated more $^1O_2$ in the activation of H_2O_2. Due to the increasing amounts of •OH and $O_2^{\bullet-}$, the increasing amount of $^1O_2$ may be generated via free radical chain reaction [51,52]. From these results, it can be concluded that sulfidation facilitates the formation of active species by the catalyst in H_2O_2 activation and subsequently improves pollutant removal, and the reasons behind this need to be further investigated.

3.4. Electron transfer capacity of catalysts

The removal discrepancies between adsorption and addition of KSCN, which can combine with Fe to cover the active site, indicates that the non-radical pathways such as electron transport are also involved in APAP degradation in the FSNC-5/H_2O_2 system (Fig. 4**a** and **S10**) [53,54]. Therefore, the I-t curve was used to analyze the electron-transfer efficiency between the catalyst and H_2O_2 or catalyst and APAP (Fig. 4**h**). After adding H_2O_2, the current of FSNC-5 decreased sharply, indicating that significant electron transfer occurs between FSNC-5 and H_2O_2. However, no significant change in the current of FNC after adding H_2O_2 indicates a little electron transfer between FNC and H_2O_2, which further verified that sulfidation effectively facilitates the electron transfer between the catalyst and H_2O_2 [38]. Furthermore, the current of both FSNC and FNC showed a slightly decreasing trend after adding APAP, suggesting that a small amount of APAP was removed by the direct electron transfer pathway. Since the electron-transfer capacity plays an important role in Fe(III) reduction and H_2O_2 activation during the heterogeneous Fenton reaction, electrochemical analysis such as cyclic voltammetric (CV), electrochemical impedance spectroscopy (EIS) and Tafel curve, were employed to evaluate the electron-transfer capacity of the catalysts before and after sulfidation. Two peaks at 0.522 V and 0.358 V of FSNC-5 in the CV curve were assigned to oxidation potential (E^{ox}) and reduction potential (E^{red}), indicating that redox reactions can occur on FSNC-5 and are sustainable for H_2O_2 activation (Fig. S11) [20]. However, only one peak at −0.308 V can be found in the CV curve of FNC, suggesting that it is hard to activate H_2O_2 sustainably. The smaller semicircle radius of FSNC in EIS compared to FNC demonstrated that FSNC-5 has lower resistance to electron transport (Fig. S12). As illustrated in Tafel polarization curves, the corrosion current of FSNC-5 was 0.655 mA, higher than that of FNC (5.68 mA), indicating the higher electron transfer performance of FSNC-5 (Fig. 4**i**) [55]. These results suggest that sulfidation modulates electron distribution, increases electron donation, and facilitates electron transfer, which promotes the activation of H_2O_2 and the production of •OH.

3.5. Reaction mechanism

3.5.1. Interfacial variations of FSNC-5 before and after the reaction

To investigate the H_2O_2 activation mechanism by FSNC-5, XRD and XPS were employed to analyze the change of Fe and S states before and after the reaction. As shown in Fig. S13, the FeS_2 in FSNC-5 was converted to $FeSO_4(H_2O)$ (PDF#74–1332) after the reaction, indicating that O atom and H_2O were adsorbed on the surface of catalysts, which could facilitate Fe and S dissolution. As shown in Fig. S14, the concentration of dissolved Fe ions increased continuously throughout the reaction process in the FSNC-5/H_2O_2 system, whereas no dissolved Fe was detected in the FNC/H_2O_2 system. Since the beginning of the reaction, the concentration of dissolved Fe has reached 3.45 mg/L, with Fe^{2+} accounting for 90.7 %. This suggests that sulfidation facilitates the dissolution of Fe and accelerates the reduction of Fe(III) by surface and dissolved S, which favors the removal of APAP by homogeneous reaction [49]. Furthermore, the intensity of Fe and S peaks in the XPS spectra decreased slightly while the intensity of O increased significantly (Fig. 5**a**), resulting from the leaching of Fe and S and the adsorption of oxygen on the surface. The contents of Fe(II) and FeS_2 were decreased while the proportion of Fe(III) increased significantly (Fig. 5**b** and Fig. S15), suggesting that a certain number of electrons were transferred from FSNC-5 to H_2O_2 [1]. Nevertheless, 45 % FeS_2 and 23 % Fe(II) imply that the electron density of the Fe active center in FSNC-5 remains at a low level. The signal intensity of S was slightly reduced without significant alteration in element status, indicating that S atoms mainly occur dissolution during the reaction (Fig. 5**c** and Fig. S16). From the O 1 s spectra, the intensity of O_{ads} and O_{latt} increased significantly, suggesting that the O derived from H_2O_2 or dissolved oxygen can easily bind with unsaturated Fe or S sites or adsorb on the surface vacancies to form new oxygenated iron sulfides morphology (Fig. 5**d** and Fig. S17). In addition, the zeta potential of FNC decreased with increasing pH value (Fig. S18). However, the zeta potential of FSNC-5 remained the positive value at pH below 8 but turned to −16.38 mV at pH=10. These results demonstrated that sulfidation induces the adsorption of a cationic layer composed of free iron ions and H^+ on the catalyst surface, which improves the surface acidity of the catalysts and facilitates H_2O_2 activation [56].

3.5.2. Electronic structure modulation by sulfidation

Furthermore, DFT calculation was used to analyze the electric structure of catalysts before and after sulfidation and charge transfer during H_2O_2 activation. According to the above results of catalyst characterization, the DFT model for FSNC-5 is presented as Fe_3C on the bottom layer and FeS_2 on the top layer (Fig. S19). The bond length of Fe-S on the catalyst surface was remarkably increased after sulfidation compared to Fe-C, suggesting that sulfidation increases the bond length (Table S4). In addition, the electron distribution was significantly reconstructed after sulfidation and the electron was enriched from internal Fe_3C to surface FeS_2 due to the electrical attraction of S atom (Fig. 5**e**) [57]. Compared to FNC, the projected density of states (PDOS) of FSNC-5 was significantly enhanced, following the d-bond center of FSNC-5 was closer to the Fermi energy level than that of FNC. The upshift d-bond center of FSNC-5 increases electron density and facilitates electron transfer from FSNC-5 to H_2O_2, suggesting that sulfidation can improve the H_2O_2 activation capacity of the catalyst (Fig. 5**f**) [42]. Furthermore, the adsorption energy (E_{ads}) of H_2O_2 on FNC and FSNC are −5.70 eV and −3.35 eV, respectively (Fig. 5**g**), suggesting that H_2O_2 can be spontaneously adsorbed on FNC and FSNC. The length of O-O ($l_{o\text{-}o}$) of adsorbed H_2O_2 on FNC and FSNC are 2.57 Å and 2.61 Å, indicating that the cleavage of O-O more prone to occur during H_2O_2 activation by FSNC [58]. Meanwhile, the Bader electron and charge density difference demonstrated that 1.041 e^- and 0.866 e^- were transferred from the surroundings of Fe on the FNC and FSNC surfaces to H_2O_2 via Fe-O and Fe-S-O bonds, respectively [7]. Notably, due to the different adsorption energies, $l_{o\text{-}o}$, and electron transfer after H_2O_2 adsorption, the O-H was firstly cleaved by FNC to form *OOH, which was easily converted to $O_2^{\bullet-}$ by dehydrogenation. Meanwhile, the O-O was directly cleaved by FSNC to form •OH, which supports the increasing •OH generated in the FSNC/H_2O_2 system. The formation of Fe-S-O indicates that S serves as an

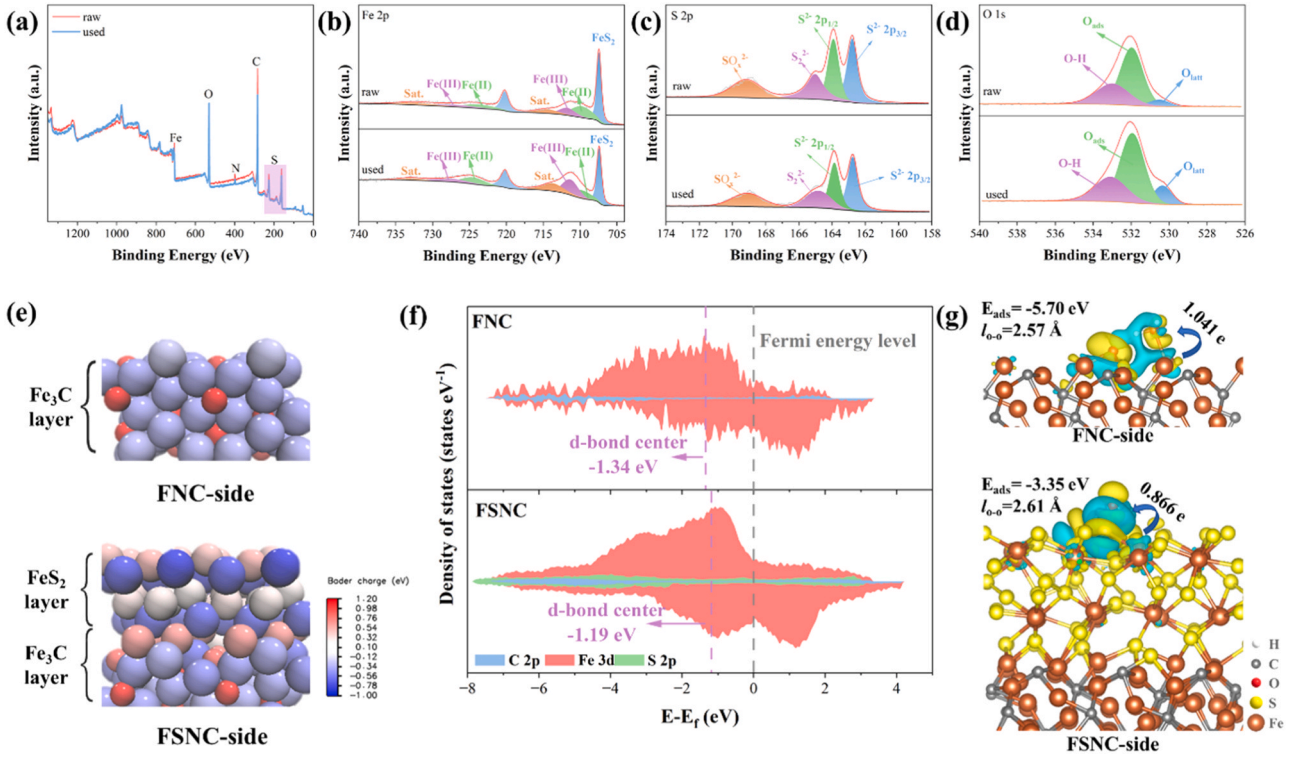

Fig. 5. The XPS full spectra (a) and precise spectrum of Fe 2p (b), S 2p (c) and O 1 s (d) of raw and used FSNC-5, the Bader charge density of FNC and FSNC-5 (e), the project density of state of FNC and FSNC-5 (f), and adsorbed energy and charge density difference of FNC and FSNC-5 during H_2O_2 activating (g).

electron donor and electron shuttle to facilitate •OH generation during H_2O_2 activation (Fig. S20 and Table S5). From the above results, it can be concluded that sulfidation improves the electron density of the Fe site on catalyst surface and modulates the adsorption state and cleavage path of H_2O_2 to form more •OH, promoting the efficient degradation of APAP.

3.5.3. The degradation of APAP

To analyze the vulnerable sites and the degradation pathway of APAP, the orbital and electron distribution of APAP was calculated. The structure of APAP and its Highest Occupied Molecular Orbital (HOMO) and Lower Unoccupied Molecular Orbital (LUMO) were shown in Fig. 6**a-c**, which demonstrated that the C atom in the benzene ring was easy to accept electrons while acetamido and hydroxyl group were easy to donate electron. Furthermore, the electrostatic potential (ESP) of APAP demonstrated that the O16 has the most negative value, which is susceptible to being attacked by electrophilic reagent (•OH) [59]. Similarly, the Fukui index (f^-, f^+, f^0 and Δf), which was used to analyze the sites more susceptible to electrophilic, nucleophilic, or radical attack, demonstrated that the O11, N13, and O16 with more negative f^- is easily attacked by radicals and occurred electrophilic reaction (Fig. 6**e-f**) [60,61]. Therefore, the O11, N13, and O16 were vulnerable sites of APAP in heterogeneous Fenton reactions. Furthermore, HPLC-MS was used to detect the intermediates generated during APAP degradation, and 11 intermediates were identified and listed in Table S6. Based on the information on intermediates and theoretical calculation, the possible degradation pathway was proposed and shown in Fig. 6**i**. The degradation intermediates of APAP can be divided into oxidation and polymerization products via radical oxidation reactions and phenolic polymerization. More specifically, the oxidation products, including P1-P5, may be converted through radical oxidation, radical addition, and open-ring reactions. The polymerization products, including P6-P11, may be converted through amide hydrolysis, polymerization, hydroxylation, and oxidation [62]. Moreover, ECOSAR was used to evaluate the toxicity of intermediates using fish, dolphins, and angels as model orgasms. The chronic and acute toxicity of degradation and opening-ring intermediates was significantly decreased while the chronic toxicity of polymerization intermediates increased in the FSNC-5/H_2O_2 system, which needs more attention (Table S7).

3.6. Application potential

The durability of catalysts and the universality of sulfidation were tested to evaluate the application potential. Almost all APAP was removed by FSNC-5 in the three cyclical experiments (Fig. S21). Furthermore, the long-term performance of the FSNC-5 was tested by column experiments. The removal of APAP was consistently above 70 % within 600 min of continuous operation, suggesting that FSNC-5 can continuously activate H_2O_2 for APAP degradation (Fig. S22). In addition, TC, SMX, phenol, and PMSO were also used as model

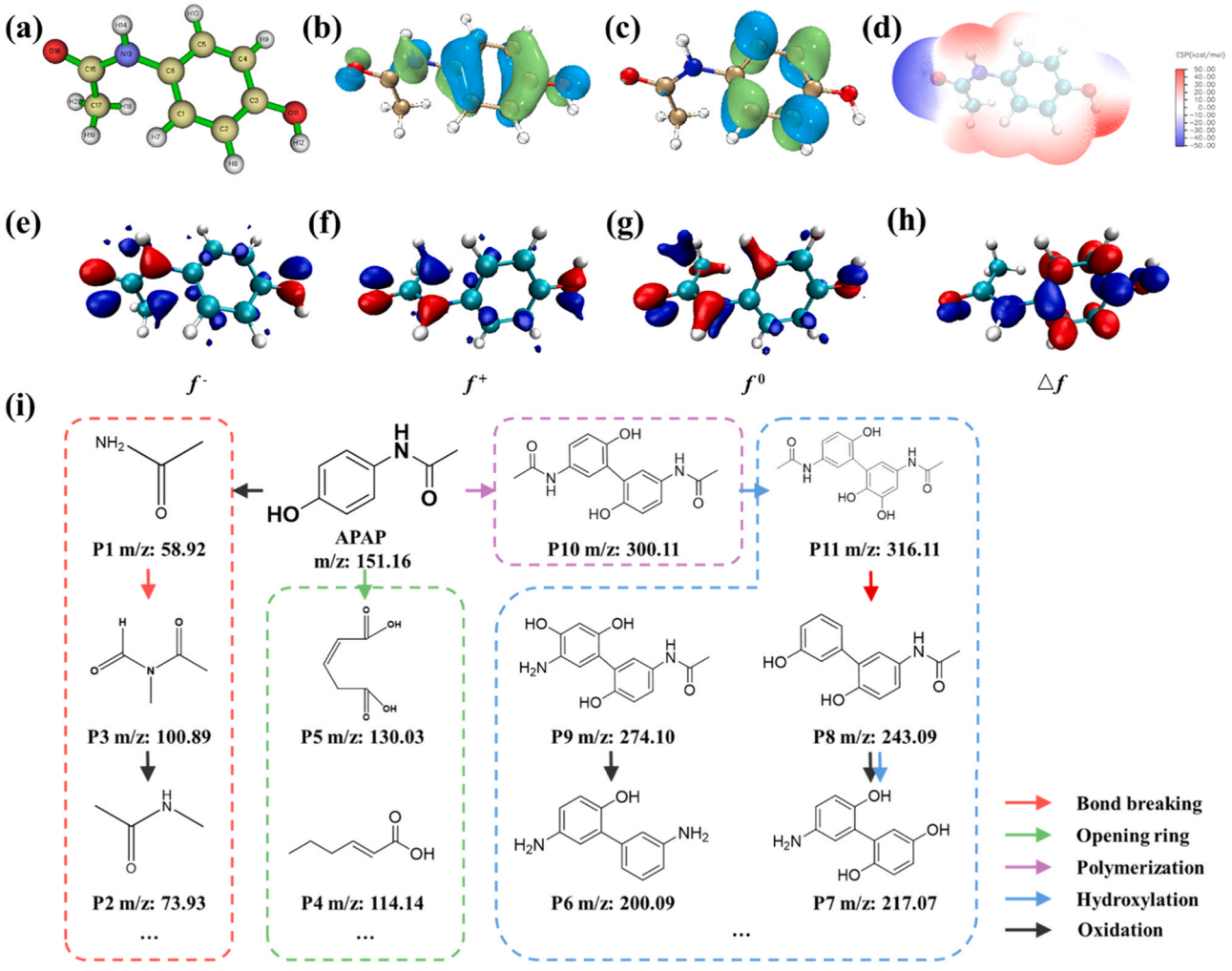

Fig. 6. The molecule structure of APAP (a) and its HOMO (b) and LUMO (c) orbital distribution, the ESP of APAP (d), Fukui index (f^- (e), f^+ (f), f^0 (g) and Δf (h)) of APAP and possible degradation pathway of APAP (i).

compounds to evaluate the universality of catalysts. Due to the major active species being •OH, which is easily affected by the water environment substrate, the removal of APAP decreased to 57.7 % and 58.4 % in river water and lake water, respectively (Fig. S23). As shown in Fig. S24, TC can be removed in the FSNC-5/H_2O_2 system in the first two minutes, while the removal of SMX and phenol were 66.3 % and 67.2 %, respectively, suggesting that the FSNC-5/H_2O_2 system showed a great universality in pollutant degradation. In addition, Fe_3O_4, a normal heterogeneous Fenton catalyst, was used to replace Fe_3C/NCT to evaluate the universality of sulfidation (Fig. S25). Only 0.3 % APAP was removed in the Fe_3O_4/H_2O_2 system, which increased to 90.8 % in the S-Fe_3O_4/H_2O_2 system. Although this performance is lower than that in the FSNC-5/H_2O_2 system, it also suggests that sulfidation can serve as an effective universal method to enhance the reactivity of heterogeneous Fenton catalysts.

4. Conclusions

In this work, we provide an effective method to enhance the heterogeneous Fenton performance of Fe_3C-based catalyst through introducing sulfidation. The k_{obs} of APAP increased 5.44-fold after sulfidation, while the H_2O_2 consumption increased from 9.3 % to 54.6 %, verifying that sulfidation improves the removal of APAP and the utilization of H_2O_2. Quenching experiment, probe experiment, and EPR results indicated that the •OH, $O_2^{\bullet-}$, and $^1O_2$ were the reactive species in the FSNC/H_2O_2 system and validated that sulfidation facilitated their production. Electrochemical analysis revealed that the electron transfer resistance was reduced and electron transfer between FSNC and H_2O_2 was enhanced after sulfidation. Theoretical calculations demonstrated that the electron density of the Fe atom on the catalyst surface was significantly increased after sulfidation, which facilitated the electron transfer from the catalyst to H_2O_2. The reduced energy gap between the d-band center and Fermi energy level further reduces the energy barriers of H_2O_2 activation. Due to the gaining electron density and the optimized electronic structure, the cleavage position of H_2O_2 was converted from O-H to O-O, causing its product converted from •OOH to •OH. These conclusions collectively elucidate the synergistic mechanism of sulfation on H_2O_2 activation and APAP degradation. In the degradation of APAP, the N and O atoms, which have higher electron density in APAP, were found to be easily susceptible to attack and degraded to amides, organic acids, and polymers. The improvement of Fe_3O_4 catalyst performance after sulfidation verifies that it is a universal measure to improve catalyst performance. In summary, this research elucidated the enhancement mechanism of sulfidation and provided a universal measure to improve the performance of heterogeneous Fenton catalysts.

CRediT authorship contribution statement

Dunyu Sun: Writing – original draft, Methodology, Investigation, Conceptualization. **Leliang Wu:** Methodology, Investigation. **Qiang Zhong:** Conceptualization. **KwangChol Ri:** Methodology. **Syed Azhar Abbas:** Writing – review & editing. **Shaogui Yang:** Writing – review & editing, Supervision, Funding acquisition, Conceptualization. **Chenmin Xu:** Writing – review & editing, Resources. **Shanshan Ding:** Writing – review & editing. **Yazi Liu:** Resources. **Zhe Xu:** Resources. **Chengdu Qi:** Resources. **Huan He:** Resources. **Shiyin Li:** Resources. **Cheng Sun:** Resources.

Declaration of Competing Interest

The authors declare that they have no known competing financial interests or personal relationships that could have appeared to influence the work reported in this paper.

Data availability

Data will be made available on request.

Acknowledgments

This work was supported by Major Projects of Jiangsu Provincial Department of Education [23KJA180004], Postgraduate Research and Practice Innovation in Jiangsu Province Program [KYCX22_1648, KYCX23_1778], High-end Foreign Expert Introduction Program [G2023014055L], the Jiangsu Provincial Key Research and Development Program [BE2023826], China Postdoctoral Science Foundation Funded Project [2023M741761], the Postdoctoral Fellowship Program of CPSF [GZC20231138], the "Kuncheng Talent" Science and Technology Innovation and Entrepreneurship Leading Talents Program in Changshu.

Appendix A. Supporting information

Supplementary data associated with this article can be found in the online version at doi:10.1016/j.apcatb.2024.124076.

References

[1] J.J. Pignatello, E. Oliveros, A. MacKay, Advanced oxidation processes for organic contaminant destruction based on the fenton reaction and related chemistry, Crit. Rev. Environ. Sci. Technol. 36 (2006) 1–84, https://doi.org/10.1080/10643380500326564.
[2] D.F. Bishop, G. Stern, M. Fleischman, L.S. Marshall, Hydrogen peroxide catalytic oxidation of refractory organics in municipal waste waters, Ind. Eng. Chem. Process. 7 (1968) 110–117, https://doi.org/10.1021/i260025a022.
[3] F. Haber, J. Weiss, W.J. Pope, The catalytic decomposition of hydrogen peroxide by iron salts, Proc. Math. Phys. Eng. Sci. 147 (1934) 332–351, https://doi.org/10.1098/rspa.1934.0221.
[4] W.C. Bray, M.H. Gorin, Ferryl ion, a compound of tetravalent iron, J. Am. Chem. Soc. 54 (1932) 2124–2125, https://doi.org/10.1021/ja01344a505.
[5] P. Zhou, W. Ren, G. Nie, X. Li, X. Duan, Y. Zhang, S. Wang, Fast and long-lasting iron(III) reduction by boron toward green and accelerated fenton chemistry, Angew. Chem. Int. Ed. 59 (2020) 16517–16526, https://doi.org/10.1002/anie.202007046.
[6] Y. Chen, C.J. Miller, T.D. Waite, Heterogeneous fenton chemistry revisited: mechanistic insights from ferrihydrite-mediated oxidation of formate and oxalate, Environ. Sci. Technol. 55 (2021) 14414–14425, https://doi.org/10.1021/acs.est.1c00284.
[7] H. Zhan, R. Zhou, P. Wang, Q. Zhou, Selective hydroxyl generation for efficient pollutant degradation by electronic structure modulation at Fe sites, Proc. Natl. Acad. Sci. U. S. A. 120 (2023) e2305378120, https://doi.org/10.1073/pnas.2305378120.
[8] H. Zhou, J. Peng, J. Li, J. You, L. Lai, R. Liu, Z. Ao, G. Yao, B. Lai, Metal-free black-red phosphorus as an efficient heterogeneous reductant to boost Fe^{3+}/Fe^{2+} cycle for peroxymonosulfate activation, Water Res. 188 (2021) 116529, https://doi.org/10.1016/j.watres.2020.116529.
[9] C. Lai, X. Shi, L. Li, M. Cheng, X. Liu, S. Liu, B. Li, H. Yi, L. Qin, M. Zhang, N. An, Enhancing iron redox cycling for promoting heterogeneous Fenton performance: a review, Sci. Total Environ. 775 (2021) 145850, https://doi.org/10.1016/j.scitotenv.2021.145850.
[10] D.B. Miklos, C. Remy, M. Jekel, K.G. Linden, J.E. Drewes, U. Hübner, Evaluation of advanced oxidation processes for water and wastewater treatment – a critical review, Water Res 139 (2018) 118–131, https://doi.org/10.1016/j.watres.2018.03.042.
[11] Y. Chen, C.J. Miller, T.D. Waite, pH dependence of hydroxyl radical, ferryl, and/or ferric peroxo species generation in the heterogeneous fenton process, Environ. Sci. Technol. 56 (2022) 1278–1288, https://doi.org/10.1021/acs.est.1c05722.
[12] N. Li, X. He, J. Ye, H. Dai, W. Peng, Z. Cheng, B. Yan, G. Chen, S. Wang, H_2O_2 activation and contaminants removal in heterogeneous Fenton-like systems, J. Hazard. Mater. 458 (2023) 131926, https://doi.org/10.1016/j.jhazmat.2023.131926.
[13] Y. Chen, C.J. Miller, R.N. Collins, T.D. Waite, Key considerations when assessing novel fenton catalysts: iron oxychloride (FeOCl) as a case study, Environ. Sci. Technol. 55 (2021) 13317–13325, https://doi.org/10.1021/acs.est.1c04370.
[14] X.-j Yang, X.-m Xu, J. Xu, Y.-f Han, Iron oxychloride (FeOCl): an efficient fenton-like catalyst for producing hydroxyl radicals in degradation of organic contaminants, J. Am. Chem. Soc. 135 (2013) 16058–16061, https://doi.org/10.1021/ja409130c.
[15] J. Wang, J. Tang, Fe-based Fenton-like catalysts for water treatment: catalytic mechanisms and applications, J. Mol. Liq. 332 (2021) 115755, https://doi.org/10.1016/j.molliq.2021.115755.
[16] P. Zhao, Y. Jiang, Z. Tang, Y. Li, B. Sun, Y. Wu, J. Wu, Y. Liu, W. Bu, Constructing electron levers in perovskite nanocrystals to regulate the local electron density for

intensive chemodynamic therapy, Angew. Chem. Int. Ed. 60 (2021) 8905–8912, https://doi.org/10.1002/anie.202100864.
[17] J. Hu, S. Wang, J. Yu, W. Nie, J. Sun, S. Wang, Duet Fe_3C and FeN_x sites for H_2O_2 generation and activation toward enhanced electro-Fenton performance in wastewater treatment, Environ. Sci. Technol. 55 (2021) 1260–1269, https://doi.org/10.1021/acs.est.0c06825.
[18] Y. Xiang, D. Yuan, E. Zhu, T. Zhao, T. Jiao, Q. Zhang, S. Tang, Efficacious reduction of ferric ions by molybdenum carbide in the peroxydisulfate Fenton-like reaction for dexamethasone degradation, ACS EST Water 3 (2023) 857–865, https://doi.org/10.1021/acsestwater.2c00609.
[19] H. Zhou, J. Peng, X. Duan, H. Yin, B. Huang, C. Zhou, S. Zhong, H. Zhang, P. Zhou, Z. Xiong, Z. Ao, S. Wang, G. Yao, B. Lai, Redox-active polymers as robust electron-shuttle co-catalysts for fast Fe^{3+}/Fe^{2+} circulation and green fenton oxidation, Environ. Sci. Technol. 57 (2023) 3334–3344, https://doi.org/10.1021/acs.est.2c07447.
[20] T. Zhang, Z. Pan, J. Wang, X. Qian, H. Yamashita, Z. Bian, Y. Zhao, Homogeneous carbon dot-anchored Fe(III) catalysts with self-regulated proton transfer for recyclable fenton chemistry, JACS Au 3 (2023) 516–525, https://doi.org/10.1021/jacsau.2c00644.
[21] Q.-Q. Huang, H.-Z. Liu, M. Huang, J. Wang, H.-Q. Yu, Ligand-assisted heterogeneous catalytic H2O2 activation for pollutant degradation: the trade-off between coordination site passivation and adjacent site activation, Appl. Catal. B 330 (2023) 122592, https://doi.org/10.1016/j.apcatb.2023.122592.
[22] Y. Gao, P. Wang, Y. Chu, F. Kang, Y. Cheng, E. Repo, M. Feng, X. Yu, H. Zeng, Redox property of coordinated iron ion enables activation of O_2 via in-situ generated H_2O_2 and additionally added H_2O_2 in EDTA-chelated Fenton reaction, Water Res 248 (2023) 120826, https://doi.org/10.1016/j.watres.2023.120826.
[23] H. Zhang, L. Li, N. Chen, H. Ben, G. Zhan, H. Sun, Q. Li, J. Sun, L. Zhang, Hydroxylamine enables rapid heterogeneous-homogeneous coupled Fenton sulfamethazine degradation on ferric phosphate, Appl. Catal. B 312 (2022) 121410, https://doi.org/10.1016/j.apcatb.2022.121410.
[24] Z. Li, Y. Huo, T. Li, S. Dong, M. Huo, G. Liu, M. Sun, Toward practical water decontaminations via peroxymonosulfate nonradical oxidation: the role of cocatalyst MoS_2 with sulfur vacancies, ACS EST Eng. 3 (2023) 1975–1985, https://doi.org/10.1021/acsestengg.3c00283.
[25] M. Huang, X. Wang, C. Liu, G. Fang, J. Gao, Y. Wang, D. Zhou, Mechanism of metal sulfides accelerating Fe(II)/Fe(III) redox cycling to enhance pollutant degradation by persulfate: metallic active sites vs. reducing sulfur species, J. Hazard. Mater. 404 (2021) 124175, https://doi.org/10.1016/j.jhazmat.2020.124175.
[26] C. Dong, J. Ji, B. Shen, M. Xing, J. Zhang, Enhancement of H_2O_2 decomposition by the Co-catalytic effect of WS_2 on the Fenton reaction for the synchronous reduction of Cr(VI) and remediation of phenol, Environ. Sci. Technol. 52 (2018) 11297–11308, https://doi.org/10.1021/acs.est.8b02403.
[27] S. Zuo, D. Li, Z. Guan, F. Yang, J. Song, H. Xu, D. Xia, H. Li, X. Li, A directional Built-in electric field mediates the electron transfer synergy mechanism of the Radical/Nonradical pathway in FeOCl-CuO, Chem. Eng. J. 430 (2022), https://doi.org/10.1016/j.cej.2021.133004.
[28] K. Zhu, W. Qin, Y. Gan, Y. Huang, Z. Jiang, Y. Chen, X. Li, K. Yan, Acceleration of Fe^{3+}/Fe^{2+}cycle in garland-like MIL-101(Fe)/MoS_2 nanosheets to promote peroxymonosulfate activation for sulfamethoxazole degradation, Chem. Eng. J. 470 (2023), https://doi.org/10.1016/j.cej.2023.144190.
[29] C. Wang, W. Zhang, J. Wang, P. Xia, X. Duan, Q. He, I. Sirés, Z. Ye, Accelerating Fe(III)/Fe(II) redox cycling in heterogeneous electro-Fenton process via S/Cu-mediated electron donor-shuttle regime, Appl. Catal. B 342 (2024) 123457, https://doi.org/10.1016/j.apcatb.2023.123457.
[30] J. Xu, A. Avellan, H. Li, X. Liu, V. Noël, Z. Lou, Y. Wang, R. Kaegi, G. Henkelman, G.V. Lowry, Sulfur loading and speciation control the hydrophobicity, electron transfer, reactivity, and selectivity of sulfidized nanoscale zerovalent iron, Adv. Mater. 32 (2020) 1906910, https://doi.org/10.1002/adma.201906910.
[31] J. Qu, Z. Li, F. Bi, X. Zhang, B. Zhang, K. Li, S. Wang, M. Sun, J. Ma, Y. Zhang, A multiple Kirkendall strategy for converting nanosized zero-valent iron to highly active Fenton-like catalyst for organics degradation, Proc. Natl. Acad. Sci. U. S. A. 120 (2023) e2304552120, https://doi.org/10.1073/pnas.2304552120.
[32] F. Gao, M. Zhang, X. Yang, S. Ahmad, J. Tang, Post-sulfidation of biochar supported nanoscale zero-valent iron with different sulfur precursors: reactivity and selectivity on tetrabromobisphenol A reduction, Chem. Eng. J. 461 (2023) 141953, https://doi.org/10.1016/j.cej.2023.141953.
[33] X. Gao, Y. Zhang, F. Li, B. Tian, X. Wang, Z. Wang, J.C. Carozza, Z. Zhou, H. Han, C. Xu, Surface modulation and chromium complexation: all-in-one solution for the Cr(VI) sequestration with bifunctional molecules, Environ. Sci. Technol. 54 (2020) 8373–8379, https://doi.org/10.1021/acs.est.0c00710.
[34] J. Li, X. Zhang, M. Liu, B. Pan, W. Zhang, Z. Shi, X. Guan, Enhanced reactivity and electron selectivity of sulfidated zerovalent iron toward chromate under aerobic conditions, Environ. Sci. Technol. 52 (2018) 2988–2997, https://doi.org/10.1021/acs.est.7b06502.
[35] H. Li, J. Zhang, K. Gu, J. Li, Sulfidation of zerovalent iron for improving the selectivity toward Cr(VI) in oxic water: involvements of FeSx, J. Hazard. Mater. 409 (2021) 124498, https://doi.org/10.1016/j.jhazmat.2020.124498.
[36] Y. Gao, W. Zhu, J. Liu, P. Lin, J. Zhang, T. Huang, K. Liu, Mesoporous sulfur-doped $CoFe_2O_4$ as a new Fenton catalyst for the highly efficient pollutants removal, Appl. Catal. B 295 (2021), https://doi.org/10.1016/j.apcatb.2021.120273.
[37] X. Tian, T. Luo, Y. Nie, J. Shi, Y. Tian, D.D. Dionysiou, Y. Wang, New insight into a Fenton-like reaction mechanism over sulfidated β-FeOOH: key role of sulfidation in efficient iron(III) reduction and sulfate radical generation, Environ. Sci. Technol. 56 (2022) 5542–5551, https://doi.org/10.1021/acs.est.2c00132.
[38] D. Sun, B. Shen, S. Yang, X. Cheng, Q. Zhong, S. Azhar Abbas, Y. Dai, Y. Liu, C. Xu, C. Qi, H. He, S. Li, Nitrogen-doped CNTs enhance heterogeneous Fenton reaction for IOH removal by FeOCl: Role of NCNTs and mechanism, Sep. Purif. Technol. 326 (2023) 124763, https://doi.org/10.1016/j.seppur.2023.124763.
[39] L. Su, Y. Li, Z. Wang, Y.-Y. Lou, Q.-Z. Zheng, Z. Wu, S.-P. Sun, Nonradical activation of Oxone over Fe-doped nitrogen carbon (Fe@NC) armor catalysts for efficient degradation of anthropogenic phenolics (p-nitrophenol, 4-chlorophenol) in groundwater matrices, Chem. Eng. J. 477 (2023) 146920, https://doi.org/10.1016/j.cej.2023.146920.
[40] H. Xu, Y. Li, D. Zhu, Z. Li, F. Sun, W. Zhu, Y. Chen, J. Zhang, L. Ren, S. Zhang, J. Zou, R.M. Laine, Synchrotron radiation spectroscopic studies of Mg^{2+} storage mechanisms in high-performance rechargeable magnesium batteries with Co-doped FeS_2 cathodes, Adv. Energy Mater. 12 (2022) 2201608, https://doi.org/10.1002/aenm.202201608.
[41] J. Shang, Y. Zhang, F. Zhou, F. Lv, F. Han, J. Lu, X. Meng, P.K. Chu, Z. Ye, J. Xing, Analysis of hazardous organic residues from sodium hydrosulfite industry and utilization as raw materials in a novel solid lubricant production, J. Hazard. Mater. 198 (2011) 65–69, https://doi.org/10.1016/j.jhazmat.2011.10.013.
[42] Y. Zhao, D. Song, X. Zhang, S. Wang, Z. Sun, C. Liu, J. Ma, Y. Ren, Regulating B-site metals in delafossite to reach efficient and selective peroxymonosulfate activation for water remediation, ACS EST Eng. 3 (2023) 2109–2121, https://doi.org/10.1021/acsestengg.3c00421.
[43] B. Wang, Y. Chen, G. Liu, D. Liu, Y. Liu, C. Ge, L. Wang, Z. Wang, R. Wu, L. Wang, Interfaces coupling of Co_8FeS_8-Fe_5C_2 with elevated d-band center for efficient water oxidation catalysis, Appl. Catal. B 341 (2024) 123294, https://doi.org/10.1016/j.apcatb.2023.123294.
[44] D. Cheng, Y. Tan, R. Ma, H. Ding, W. Liao, K. He, R. Sun, H. Ni, F. He, Degradation of nitrobenzene by mackinawite through a sequential two-step reduction and oxidation process, Environ. Sci. Technol. 57 (2023) 19827–19837, https://doi.org/10.1021/acs.est.3c07152.
[45] L. Gao, Y. Guo, J. Zhan, G. Yu, Y. Wang, Assessment of the validity of the quenching method for evaluating the role of reactive species in pollutant abatement during the persulfate-based process, Water Res 221 (2022) 118730, https://doi.org/10.1016/j.watres.2022.118730.
[46] H. Dong, Y. Li, S. Wang, W. Liu, G. Zhou, Y. Xie, X. Guan, Both Fe(IV) and radicals are active oxidants in the Fe(II)/peroxydisulfate process, Environ. Sci. Technol. Lett. 7 (2020) 219–224, https://doi.org/10.1021/acs.estlett.0c00025.
[47] L. Chen, J. Duan, P. Du, W. Sun, B. Lai, W. Liu, Accurate identification of radicals by in-situ electron paramagnetic resonance in ultraviolet-based homogenous advanced oxidation processes, Water Res 221 (2022) 118747, https://doi.org/10.1016/j.watres.2022.118747.
[48] Q. Zhong, Y. Sun, C. Xu, Y. Li, D. Sun, L. Wu, S. Yang, Y. Liu, C. Qi, Z. Xu, H. He, S. Li, Z. Wang, S. Wang, Fe_xSe_y@C superlattice nanocrystals for peroxymonosulfate activation: intrinsic nature of Fe spin state, Appl. Catal. B 339 (2023) 123113, https://doi.org/10.1016/j.apcatb.2023.123113.
[49] K. Hou, Z. Pi, F. Chen, L. He, F. Yao, S. Chen, X. Li, H. Dong, Q. Yang, Trace-dissolved S(-II) triggers the Fe(III)-activated H_2O_2 process for organic pollutant degradation by promoting the Fe(III)/Fe(II) cycle: kinetics, toxicity, and mechanisms, ACS EST Eng. 2 (2022) 2174–2186, https://doi.org/10.1021/acsestengg.2c00185.
[50] C. Beauchamp, I. Fridovich, Superoxide dismutase: improved assays and an assay applicable to acrylamide gels, Anal. Biochem. 44 (1971) 276–287, https://doi.org/10.1016/0003-2697(71)90370-8.
[51] Z. Yang, J. Qian, A. Yu, B. Pan, Singlet oxygen mediated iron-based Fenton-like catalysis under nanoconfinement, Proc. Natl. Acad. Sci. U. S. A. 116 (2019) 6659–6664, https://doi.org/10.1073/pnas.1819382116.
[52] C. Dong, Y. Yang, X. Hu, Y. Cho, G. Jang, Y. Ao, L. Wang, J. Shen, J.H. Park, K. Zhang, Self-cycled photo-Fenton-like system based on an artificial leaf with a solar-to-H_2O_2 conversion efficiency of 1.46, Nat. Commun. 13 (2022) 4982, https://doi.org/10.1038/s41467-022-32410-0.
[53] Q.-Y. Wu, Z.-W. Yang, Z.-W. Wang, W.-L. Wang, Oxygen doping of cobalt-single-atom coordination enhances peroxymonosulfate activation and high-valent cobalt–oxo species formation, Proc. Natl. Acad. Sci. U. S. A. 120 (2023) e2219923120, https://doi.org/10.1073/pnas.2219923120.
[54] Q. Zhong, Y. Sun, S. Wu, C. Xu, S. Yang, Y. Liu, D. Sun, B. Yang, Y. Dai, C. Qi, Z. Xu, H. He, S. Li, S. Wang, Uniformed core-shell $FeSe_{2+x}$@C nanocube superlattices for Fenton-like reaction: coordinative roles of cation and anion, Appl. Catal. B 325 (2023) 122357, https://doi.org/10.1016/j.apcatb.2022.122357.
[55] Z. Fang, J. Qi, W. Chen, L. Zhang, J. Wang, C. Tian, Q. Dai, W. Liu, L. Wang, Defect engineering-mediated Co_9S_8 with unexpected catalytic selectivity for heterogeneous Fenton-like reaction: Unveiling the generation route of $^1O_2$ in V_S active site, Appl. Catal. B 338 (2023) 123084, https://doi.org/10.1016/j.apcatb.2023.123084.
[56] Q. Yan, C. Lian, K. Huang, L. Liang, H. Yu, P. Yin, J. Zhang, M. Xing, Constructing an acidic microenvironment by MoS_2 in heterogeneous Fenton reaction for pollutant control, Angew. Chem. Int. Ed. 60 (2021) 17155–17163, https://doi.org/10.1002/anie.202105736.
[57] W. Li, L. Jin, S. Jiang, Y. Liu, Electrified nitrogen-doped MXene membrane electrode for micropollutants decontamination via peroxymonosulfate activation, ACS EST Eng. (2023), https://doi.org/10.1021/acsestengg.3c00222.
[58] B. Zeng, L. Long, Y. Chen, Z. Liu, L. Luo, Q. Shao, P. Xie, J. Ma, New insights into the FeO/peroxymonosulfate process for organics removal: the synergistic effect of radicals and Fe(IV), ACS EST Eng. 3 (2023) 1886–1897, https://doi.org/10.1021/acsestengg.3c00260.

[59] J. Zhang, T. Lu, Efficient evaluation of electrostatic potential with computerized optimized code, Phys. Chem. Chem. Phys. 23 (2021) 20323–20328, https://doi.org/10.1039/D1CP02805G.
[60] R.G. Parr, W. Yang, Density functional approach to the frontier-electron theory of chemical reactivity, J. Am. Chem. Soc. 106 (1984) 4049–4050, https://doi.org/10.1021/ja00326a036.
[61] T.L. Rong, Fu Fei-Wu Chen, Comparing methods for predicting the reactive site of electrophilic substitution, Acta Phys. -Chim. Sin. 30 (2014) 628–639, https://doi.org/10.3866/pku.Whxb201401211.
[62] V.K. Parida, S.K. Srivastava, S. Chowdhury, A.K. Gupta, Facile synthesis of 2D/0D Bi_2O_3/MnO_2 Z-scheme heterojunction for enhanced visible light-assisted photocatalytic degradation of acetaminophen, Chem. Eng. J. 472 (2023) 144969, https://doi.org/10.1016/j.cej.2023.144969.